ACS Energy LETTERS

http://pubs.acs.org/journal/aelccp

Negative Transient Spikes in Halide Perovskites

Enrique Hernández-Balaguera* and Juan Bisquert

Cite This: ACS Energy Lett. 2022, 7, 2602−2610

Read Online

ACCESS | Metrics & More | Article Recommendations | Supporting Information

ABSTRACT: The internal crossfire of ionic and electronic effects in perovskite devices forms a complex analysis problem that has not been fully solved yet. Specifically, halide photovoltaic perovskites show a photoinduced ionic inductance behavior in current transient measurements, evidenced by ubiquitous negative spikes. Here, we provide a consolidated interpretation of these observed chemical mechanisms by independent measurement routes (frequency and time domain) in order to solve an elusive topic in the development of perovskite solar cells for more than a decade. From this operational pathway, we specifically study the light-dependent negative overshoot photocurrent phenomena in the time-domain discharge of the chemical inductor, which is a transversal mechanism found in a multitude of chemical, biological, and material systems. Our results establish a general framework to understand the inductive transient effects observable in new and important applications of halide perovskites, capable of emulating the electrical activity of neurons and synapses when acting as memristors.

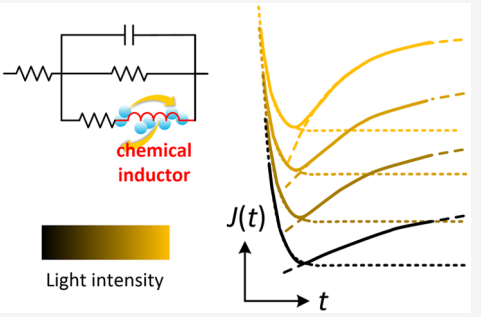

Despite impressive progress of the halide perovskite solar cells and a multitude of related devices like light emitting diodes, photodetectors, and memristors, important aspects of the kinetic operation of these photovoltaic and electronic systems have not been well-understood yet. The main factor of complexity is that these systems are composed of dynamics of multiple electronic and ionic carriers that show well-separated time scales but interact with each other.[1−3] Along these years in which the photovoltaic perovskites have emerged as the new solar power's next star material, there have been observed rather irregular and intriguing features in the analysis of their transient dynamics.

One of the most relevant and unsolved questions in this regard, remaining still under a lively debate, is that the current transient dynamics often show a photoinduced negative spike, in which the response decreases to a minimum value before raising to the final equilibrium state.[4−8] This anomalous feature has been explained mainly by an effect where the applied stimuli creates a transient ionic configuration, in which an inverted polarization produces an electrical field that causes the initial negative current.[7] While the overall shape of transients is well-described by a time-dependent drift-diffusion model, the negative overshoots just after the step change and at longer time cannot be described by such a model approach. It has been also suggested that the origin of the apparent "inverted responses" is the phase-delayed electronic injection currents, modified by a slow ionic process that changes the sign in the relaxation functions.[9] The negative spikes and the ulterior transient responses are also real features in electrochemical, biological, and semiconductor systems, which have already been qualitatively correlated with inductive mechanisms, of chemical origin and not electromagnetic, evidenced via impedance spectroscopy (IS).[10−13] In this sense, ionically gated transistors have been proposed to capture both apparent capacitive and inductive behavior in perovskite solar cells.[14] However, even though the negative time transients have been interpreted from a physical perspective, the situation is far from being well-formulated through an analytical representation of photocurrent dynamics in the time domain, adequately correlated with classical frequency-resolved measurements.

In this paper, we describe the negative overshoots in the time photocurrent transients in terms of the discharge of the inductive component extracted from the impedance. The ubiquitous spikes are a direct consequence of the presence of the chemical inductor, "the heart of slow dynamical behavior", not only in photovoltaic perovskites but also in a multitude of materials.[10] As explained in detail later in this Letter, the chemical inductor is a general denomination for a class of dynamical models often based on chemical reaction that

Received: May 30, 2022
Accepted: July 12, 2022
Published: July 18, 2022

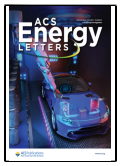

https://doi.org/10.1021/acsenergylett.2c01252
ACS Energy Lett. 2022, 7, 2602−2610

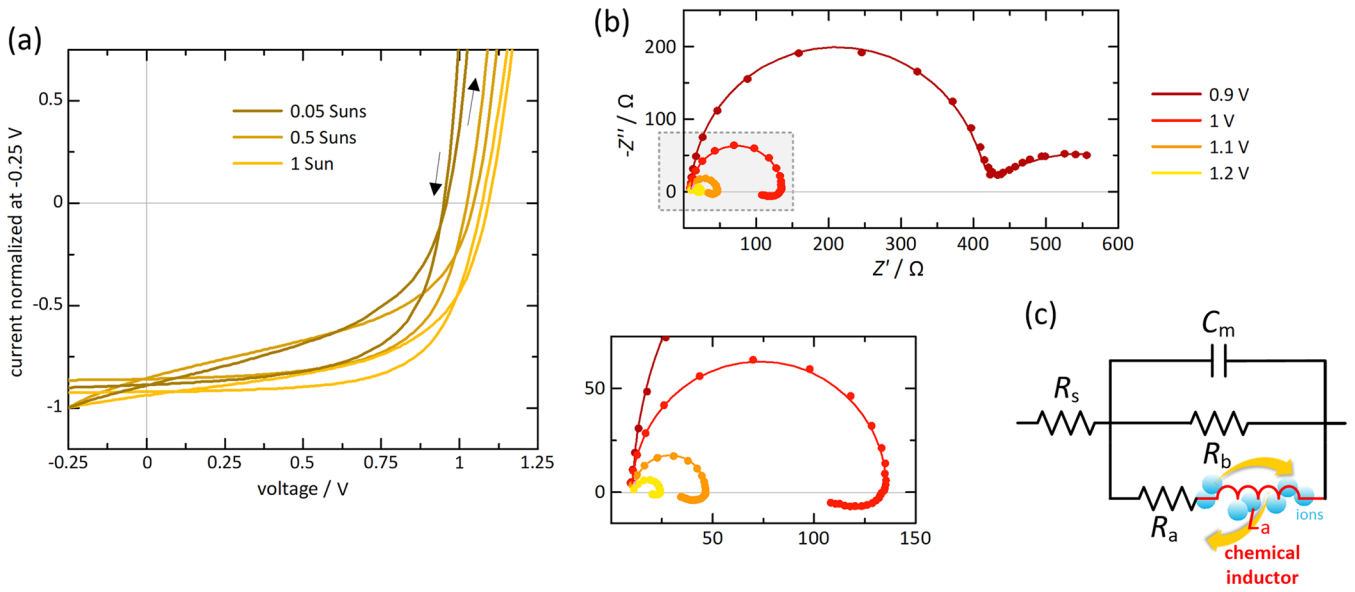

Figure 1. (a) $J-V$ curves as a function of illumination intensity normalized at −0.25 V. (b) Complex plane plot representation of the impedance spectra operated under different applied voltages and at 0.05 Suns. The frequency range is from 1 MHz to 1 Hz. Inset in (b) shows an expanded view of the positive loops of impedance spectra. (c) Equivalent circuit used for fitting the impedance data of perovskite solar cells with the chemical inductor.

produces a formal inductive response in impedance and transients without an underlying electromagnetic (induction) effect. A relevant example of the multidisciplinary application of the chemical inductor is the action potential of neurons in electrophysiology, which propagate the information in the nervous system.[15] In this signal, the return to equilibrium of the membrane voltage overcomes the zero line in the negative spike and produces a refractory period.[16] In that regard, an in-depth analysis of transient effects for recent memory applications of metal halide perovskites is especially necessary, e.g., the artificial synapses in neuromorphic computation.[17−19]

There are many examples in the literature of halide perovskites where the negative spikes may be an effect of starting in a far from equilibrium situation, either by purposeful pretreatment or by absence of a resting time.[8] While previous analysis in photovoltaic perovskites relies on specific modelistic interpretations for each separate observation (ion diffusion, interfacial barriers, polarization, etc.), here we demonstrate the correspondence of independent techniques facilitated by the interpretation framework of the chemical inductor. We show that the transient spike occurs for well-equilibrated samples, and the results of impedance measurements and photocurrent transient decays provide the same parameters. This match will enable a rational characterization for perovskite devices in a consistent and reproducible manner, since the parameters obtained in equilibrium from the spectroscopic response can be separately investigated, and they account for the transient properties. Our work can also form the basis for an adequate interpretation of unexpected phenomena observed in very useful methods, such as time-domain transient measurements of the photocurrent (TPC), photovoltage (TPV), and ion-drift.[4−6,20−22] The frequent negative transient spikes are important features that need to be better understood for the operation of new halide perovskite applications as photodetectors and power electronic components.

The "mixed" transient dynamics, caused by the crossfire of capacitive and inductive mechanisms, have been regularly observed in perovskite solar cells, giving rise, among other unique phenomena, to inverted $J-V$ hysteresis.[9,23,24] To establish the strengths of our model for the description of these atypical transient phenomena, we have analyzed devices with a near-ideal electrical behavior (negligible dispersive effects)[25] under varying voltage/illumination conditions. The proposed layer structure consists of the following configuration: FTO/c-TiO_2/m-TiO_2/perovskite/spiro-OMeTAD/Au, where the active layer exhibits a composition based on Rb/Cs/MA/FA/Pb/I/Br. Here, we prepared these quadruple-cation perovskite solar cells, with the nominal formula $Rb_{0.05}Cs_{0.05}MA_{0.15}FA_{0.75}Pb_{1.05}(I_{0.95}Br_{0.05})_3$, following a similar method to that of refs 26 and 27. The champion device yielded a power conversion efficiency (PCE) of about 19.1%, with an open-circuit voltage V_{oc} of 1.11 V, short-circuit photocurrent density J_{sc} of 22 mA/cm^2, and fill factor (FF) of 78%.

In Figure 1a, we show the normalized current−voltage curves for a representative photovoltaic device measured under various light illuminations applying a sweep rate of 10 mV/s, starting with a forward sweep and directly continuing with a reverse scanning. The resulting waveforms exhibit considerable similarities (overall shape of $J-V$ curves, marked by the transition from regular to inverted hysteresis[28]) and slight differences (relative scale of the "bumps") between them. The characteristic crossing point in the mixed hysteresis behavior of $J-V$ curves shifts to lower voltage states as light intensity decreases, which can be detected by IS as the transition from capacitive to inductive mechanisms in the slow response.[29]

From the central assumption that the hysteresis type (regular or inverted) depends on the long-time-scale electrical properties of the device, we first develop frequency-dependent measurements around V_{oc}.[30] The impedance spectra at low light intensity (0.05 Suns) are illustrated in Figure 1b, where it is possible to easily visualize that the low-frequency capacitive semicircle collapses below the real impedance axis in the presence of high dc voltages, drawing a electrically enhanced and chemical inductive loop that is well-documented from the zoomed-in view of the Nyquist plots obtained at high voltages. Note that, in the inset of Figure 1b, we also show the fitting of

https://doi.org/10.1021/acsenergylett.2c01252
ACS Energy Lett. 2022, 7, 2602−2610

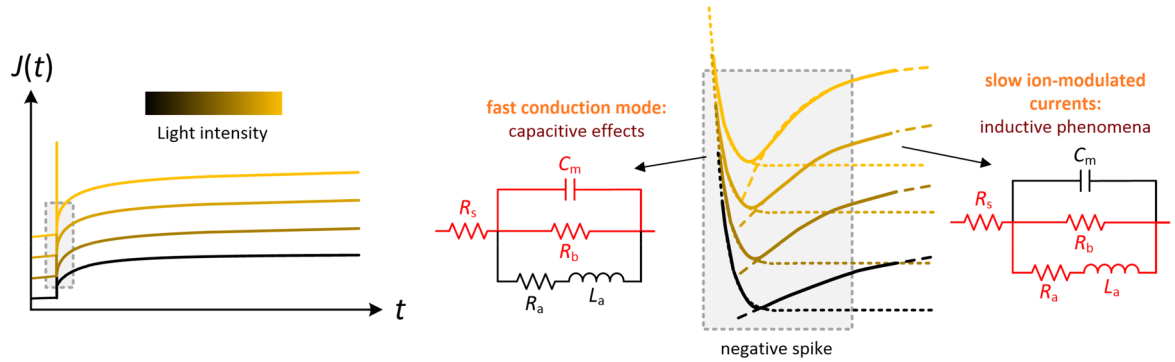

Figure 2. Inductive time-dependent current-density response of chemical origin under a forward stepwise-J−V scan for different light intensities. The left panel indicates the overall evolution of the signal described by eq 9. The inset, shown in the right panel, indicates the early time response, decomposed into an initial capacitive discharge (eq 5) and a transition, marked by the undershoot (eq 11), to the inductive control (eq 7). The active part of the equivalent circuit is highlighted in red in each fragment.

the IS data with the equivalent circuit of Figure 1c that attributes the slow inductive component to ion-controlled electronic dynamics at the interface. This equivalent circuit, containing a chemical inductor, is derived below from a very general dynamical framework, and the IS characteristics of this model are amply described in the Supporting Information and specifically summarized in the illustration of Figure S1. The impedance data at higher illumination (0.5 and 1 Sun) are similar but with a more evident chemical inductance (see below the repercussions on negative overshoots).

The physical basis for the model is shown in Figure 2. Here, we analyze the time transient current response $J(t)$ to a step stimulation, $v(t) = V_0 + \Delta V u(t)$, where V_0 is the initial voltage value and $u(t)$ is the unit step function (0 for $t < 0$ and 1 for $t > 0$). Without a loss of generality, we consider that the increment ΔV is a small positive quantity (forward sweep by using a linear control) and V_0 represents a constant high voltage value for stabilizing the electrical properties of the perovskite device to a safe current-density value, at $t = 0^-$, in the inductive region of the J−V curve. At short time scales ($t \to \tau_{ST}$), the total current flowing through the device is used to charge the dominant capacitance of the perovskite material (C_m), either dielectric or interfacial. The transition from the capacitive regime to inductive mechanisms emerges at long time scales ($t \to \tau_{LT}$), and the conduction current may be extracted from the contacts rapidly (via recombination resistance, R_b) or slowly through an ion modulated current, $J_L(t)$, when the output approaches the steady-state level. Therefore, the model can be described by the following fast−slow relaxation equations

$$\tau_{ST}\frac{dJ(t)}{dt} = \frac{\Delta V}{R_b} - J(t) + J_L(t) \quad (1)$$

$$\tau_{LT}\frac{dJ_L(t)}{dt} = \frac{\Delta V}{R_a} - J_L(t) \quad (2)$$

where

$$\tau_{ST} = R_s C_m \quad (3)$$

$$\tau_{LT} = \frac{L_a}{R_a} \quad (4)$$

and $J_L(t)$ represents the current density through the chemical inductor L_a; that is, the "slow channel" that models an electronic current that depends on ionic displacement. The initial conditions are $J(0^-) = V_0{}^{(R_a + R_b)}/_{R_a R_b}$ and $J_L(0^-) = {}^{V_0}/_{R_a}$. Remember that we consider, from our experience with perovskite measurements, that $R_a, R_b \gg R_s$ (the series resistance is negligibly small and ideally zero). As in impedance analysis, the dynamical behavior of perovskite devices involves strongly separated processes, $\tau_{LT} \gg \tau_{ST}$, and thus, the combined relaxation process $J(t)$ can be analyzed separately, being the slow one the dominant mechanism. In effect, the first two channels in eq 1 associated to C_m and R_b are "fast" in the sense that the time constant τ_{ST}, based on electronic transport mechanisms, is much shorter than the numerical value that quantifies the inertia of the slow adaptation or recovery current, τ_{LT}.

Next, we will obtain, from a physical analysis of the circuit under study, the solution of the coupled dynamical equations that in turn describe the equivalent model of the linear impedance (see Supporting Information). Network analysis and synthesis[31] reveal that "the fast conduction mode of the perovskites" can be described, under small-signal conditions, according to the following relationship

$$\Delta J(t) = \frac{\Delta V}{R_b} + \frac{\Delta V}{R_s}\exp\left[-\frac{t}{\tau_{ST}}\right], \quad t \to \tau_{ST} \quad (5)$$

where the active elements, in this short time scale, have been highlighted in red, together with the exponential decay for different light illuminations in Figure 2. Note that, for convenience, the transient dynamics have been stated explicitly in terms of photocurrent shifts because $J(0^-)$ corresponds to a different steady-state level, uncorrelated with impedance measured under bias voltage V_0.

At the instant in which the ionic inductance emerges (when t and τ_{LT} are comparable in value), it starts an exponential rise toward a new steady state which is mathematically expressed as

$$J(\infty) = (V_0 + \Delta V)\frac{R_a + R_b}{R_a R_b} \quad (6)$$

when, in practice, $t \gg \tau_{LT}$. Thus,

$$\Delta J(t) = \frac{\Delta V}{R_a}\left(\frac{R_a + R_b}{R_b} - \exp\left[-\frac{t}{\tau_{LT}}\right]\right), \quad t \to \tau_{LT} \quad (7)$$

It represents the "slow process" in the perovskites, due to the presence of ions at the interfaces, that delays $J(t)$.[10,19] Assuming that $t \ll \tau_{LT}$ (short time scale of the governing

https://doi.org/10.1021/acsenergylett.2c01252
ACS Energy Lett. 2022, 7, 2602−2610

transient term), the first two nonvanishing terms in the Maclaurin series of exponential function are considered: $\exp[-t/\tau_{LT}] = 1 - t/\tau_{LT}$.[32] Eq 7 can be approximated by

$$\Delta J(t) = \Delta V\left(\frac{t}{L_a} + \frac{1}{R_b}\right),\ t \ll \tau_{LT} \tag{8}$$

It follows that the initial interactions of mobile ions with contacts, evidenced by ionic currents in this time window, will be almost linear, governed by the slope of the exponential curve at the instant just after the trend change, which is proportional to $1/L_a$.

Using eqs 5 and 7, we can obtain a reasonable approximation of the overall transient response $\Delta J(t)$ due to the "small excursion" of voltage ΔV during a stepwise-J−V scan

$$\Delta J(t) = \frac{\Delta V}{R_s}\exp\left[-\frac{t}{\tau_{ST}}\right] + \frac{\Delta V}{R_a}\left(\frac{R_a + R_b}{R_b} - \exp\left[-\frac{t}{\tau_{LT}}\right]\right) \tag{9}$$

which is approximately equal to the result obtained from the inverse Laplace transformation of the linear impedance. The first term in eq 9 represents the response to the externally applied voltage (fast effect), to which, on the other hand, a second term is added to model the additional current due to redistribution of ions (slow process) that delays the overall current. Under certain conditions (e.g., high values of potential and light intensity), R_a and R_b can become on the same order as R_s.[9,24,29,33] This last feature has not been previously described in our theoretical model, but it can be easily deduced from the current of each circuit branch, as shown in the Supporting Information. To illustrate our theoretical background, we will consider indistinctly eq 9, and the underlying numerical approximations, and/or eqs S10−S13 depending on the scenario.

In the same sense of impedance analysis, small-amplitude transient measurements were performed in the "chemical inductance region". Figure 3a shows the measured results of the representative experiment at low light intensity. The shape of the time transients is quite similar to that predicted theoretically (*cf.* Figure 2), exhibiting well-separated time scales: initial fast decays (based on capacitive phenomena) and long tails, consisting of relatively slow adaptative rises (low frequencies in impedance analysis), dominated by the chemical inductive features due to ionic effects. The evolution of $\Delta J(t)$ indicates that the inductive currents of chemical origin increase with the applied voltage, changing more dramatically the initial fast decay dynamics of the photocurrents.

With a little attention, one can also see that the current responses, constituted by a combination of relaxation processes, exhibit ubiquitous undershoots (or "negative overshoots"), which currently generate some doubts on the transient dynamics in perovskite solar cells.[9,10,34] The "loss in amplitude" Δj of time transients can be obtained as

$$\Delta j = \frac{\Delta V}{R_b} - \Delta J(\infty) = -\frac{\Delta V}{R_a} \tag{10}$$

where, thus, this critical value in transient analysis can be easily predicted from impedance measurements, i.e., from the intermediate and low cutoff frequencies in complex plane plots (refer to Supporting Information). Note that Δj is independent of the values of R_s and R_b. In control theory, it is common to use the maximum percent overshoot when the steady-state value differs from 1.[35] The magnitude of the minimum value (maximum undershoot) in the time transients is therefore calculated as measured from the steady-state values

$$M_p = \frac{\Delta j}{\Delta J(\infty)} \times 100\% = -\frac{R_b}{R_a + R_b} \times 100\% \tag{11}$$

at the instant

$$t_p = \frac{\ln\left(\frac{R_s^2 C_m}{L_a}\right)}{\frac{1}{\tau_{LT}} - \frac{1}{\tau_{ST}}} \tag{12}$$

obtained by differentiating $\Delta J(t)$ (eq 9) with respect to time and letting this derivative equal zero, i.e., $d[\Delta J(t)]/dt|_{t=t_p} = 0$. The solution is the time required for the transient response to reach the negative spike.

Importantly, the experimental results obtained (see Figure 3a) displayed good qualitative and quantitative agreement with the mathematical model and the inductive loops found by IS

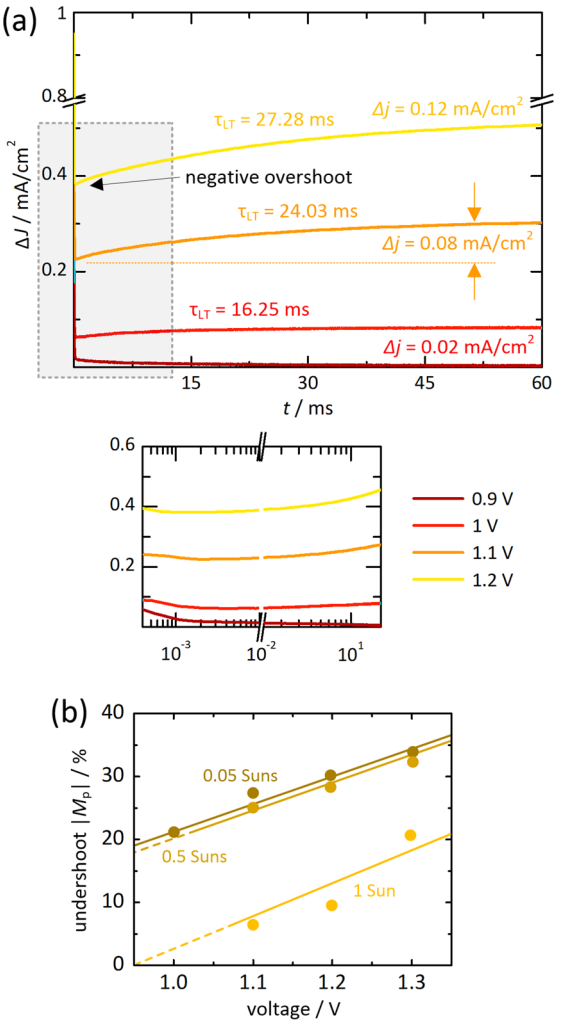

Figure 3. (a) Evolution of the experimental photocurrents over 60 ms following a jump of ΔV = 10 mV from different dc voltages at 5 mW/cm². Inset shows a zoomed-in view of the negative transient spikes for sufficiently short times in logarithm-scaled times representation. (b) Voltage dependence of the negative overshoots (undershoots) found, under different light intensities, from time transients.

https://doi.org/10.1021/acsenergylett.2c01252
ACS Energy Lett. 2022, 7, 2602−2610

Table 1. Values Calculated from the Fittings of the IS Data and Time Transients Shown in Figures 1 and 3, under Different Bias dc Voltages and at 0.05 Suns

measurement method	bias voltage (V)	L_a (H cm^2)	τ_{LT} (ms)	Δj (mA cm^{-2})	M_p (%)	t_p (μs)
impedance spectroscopy	1	9.62	19.47	0.02	−21.64	5.09
	1.1	1.46	23.61	0.09	−27.79	4.84
	1.2	0.82	30.36	0.15	−29.02	6.21
transient analysis	1	10.94	16.25	0.02	−20.53	7.18
	1.1	1.98	24.03	0.08	−26.08	5.72
	1.2	1.03	27.28	0.12	−30.77	6.14

(indicated in Table 1). Before proceeding further, it is necessary to point out that the change of transient dynamics, from a continuous decay to a "mixed" dynamics with a positive transient in current at long time scales, via ionic charge redistribution, coincides with the rotation of the low-frequency arc in the impedance spectra (Figure 1b).[9] From the inset of Figure 3a (short-time behavior of current transients), it is possible to visualize that the relaxation processes exhibit more prominent undershoots as the initial dc voltage increases, which is closely related with the value of the chemical inductance of IS. Note that values of τ_{LT}, Δj, M_p, and t_p corresponding to impedance indicated in Table 1 were obtained from eqs 4, 10−12, or S15 and S17−S19. The ratio of the two resistances R_a and R_b (or R_s+R_b and R_{dc} without numerical approximations), easily identifiable by impedance spectra (refer to Figure 1b), plays a key role in the structure of the time transients and, more particularly, in the value of the negative overshoots (see eq 11). Values of M_p, obtained from impedance measurements and transient experiments, are of the same order of magnitude in both cases, providing an excellent coincide for all applied voltages.

To further quantify the negative spikes, Figure 3b plots M_p obtained from time transients carried out at high voltages under different light intensities. It can be seen that the devices present practically a parallel behavior with a "delayed increase" of the transient current undershoot when increasing the voltage. At high illuminations (with the simultaneous increase of electronic charge density by injection and photogeneration), the impedance spectra, with non-negligible external ohmic effects, possess slight but additional physical characteristics that need to be described more precisely by a more general model that incorporates an interfacial charging capacitance.[34,36−38] To such an end, a reformulation of our theoretical and experimental study is required that is beyond the scope of this work.

In this paper, we have emphasized the correlation of the capacitive−inductive features of halide perovskite solar cells in the time and frequency domains. We would like to further consider the physical interpretation of the results. We introduce a general structure of a conduction−polarization system that is slowed down by an internal process with a memory effect.[39] The voltage across the device is $u(t)$ (do not confuse with the Heaviside step function), the total current is $J(t)$, i.e., $u(t) = v(t) - J(t)R_s$, where $v(t)$ is the external voltage, and $x(t)$ is an additional internal variable. The system is described by the nonlinear coupled dynamical equations

$$J(t) = C_m \frac{du(t)}{dt} + \frac{1}{R_I} f(u, x) \tag{13}$$

$$\tau_k \frac{dx(t)}{dt} = g(u, x) \tag{14}$$

The current $J(t)$ is composed of at least two branches according to eq 13: a capacitive charging with C_m and a conduction channel of conductivity function $f(u,x)$ and resistance scale parameter R_I. Both R_I and C_m are considered positive constants. The slow recovery variable $x(t)$ responds to the changes by a voltage-driven adaptation function $g(u,x)$ (see eq 14), with a characteristic time $\tau_k > 0$. To describe a solar cell device, the photocurrent can be added to eq 13.

To calculate the impedance, we consider the small-signal expansion, where small perturbation quantities are denoted by a tilde. Next, we take the Laplace transform, $^{d}/_{dt} \rightarrow s$ ($s = j\omega$), obtaining

$$\hat{J} = j\omega C_m \hat{u} + \frac{1}{R_I} f_u \hat{u} + \frac{1}{R_I} f_x \hat{x} \tag{15}$$

$$\tau_k j\omega \hat{x} = g_u \hat{u} + g_x \hat{x} \tag{16}$$

$$Z(s) = \frac{\hat{u}}{\hat{J}} = \left(sC_m + \frac{1}{R_b} + \frac{1}{R_a + sL_a} \right)^{-1} \tag{17}$$

In effect, we have shown previously that the impedance model of eqs 15 and 16 is that of Figure 1c.[10,39] The equivalent circuit contains the capacitor C_m, two resistances, R_b and R_a, and the inductor L_a, defined as

$$R_b = \frac{R_I}{f_u} \tag{18}$$

$$R_a = -\frac{R_I g_x}{f_x g_u} \tag{19}$$

$$L_a = \frac{R_I \tau_k}{f_x g_u} \tag{20}$$

As shown previously, the model of eqs 13 and 14 always gives the R_aL_a branch that forms a chemical inductor.[10] This result shows the universal nature of Figure 1c in terms of a fast−slow dynamical conducting system, in which the slow variable is voltage-controlled. The combination of eqs 13 and 14, with an enormous span of possibilities according to the interpretation of $x(t)$ and the nonlinear functions $f(u,x)$ and $g(u,x)$ in systems like corrosion, biological neurons, and solar cells,[11] explains the impedance spectra with an arc that enters the fourth quadrant based on a general dynamical structure, without assuming a capacitance that has a negative sign.[13] We comment in passing that the chemical inductor is not related to the chemical capacitance that describes a physical model, in which charge accumulation occurs by the increase of the chemical potential.[40]

In the field of halide perovskite solar cells, the presence of negative capacitances has featured strongly since the early

https://doi.org/10.1021/acsenergylett.2c01252
ACS Energy Lett. 2022, 7, 2602−2610

investigations,[24,33,40−42] and different explanations have been adopted to explain such features, such as the physical surface polarization model (SPM),[37,43] the changing environment of ions when their occupation at the double layer is modified by the applied voltage,[6,44,45] and the modulation of electron/hole conduction or recombination currents.[9,14,46−51] The general idea behind most of these models is based on the combination of ionic and electronic phenomena that robustly determine the dynamic response. There is an ionic reorganization determined by a slow time constant that influences the electronic current. These explanations are in agreement with the general structure of the chemical inductor generally described by eqs 13 and 14.

In the Supporting Information, we analyze in detail the impedance models suggested to explain inductive loops in perovskite solar cells. The model of Ghahremanirad et al.[37] is based on a surface polarization concept.[43] As an example of the application of the SPM, Figure S2 shows the impedance response of $MAPbBr_3$ devices with and without lithium treatment at the electron-selective layer (ESL).[24] A surface voltage V_s, associated with the interfacial barrier, responds slowly to ionic reorganization and influences electronic recombination. This mechanism follows the rule of the chemical inductor, and indeed, the resulting equivalent circuit shown in Figure 4a shows the inductive line. The model of

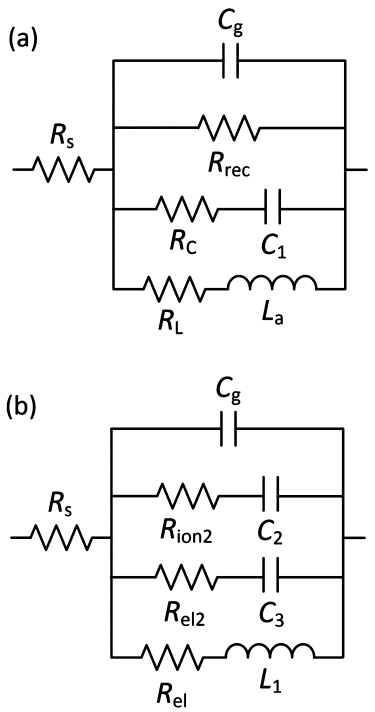

Figure 4. Equivalent circuit models that explain inductive loops. (a) Ghahremanirad et al.[37] (b) Moia and co-workers.[14]

Moia and co-workers[14] introduces a current dependence on an ionic voltage, using the image of a metaphorical transistor to describe the surface recombination control by a surface potential determined by ionic properties. The result of this study is shown in Figure 4b. Both impedance models give almost identical results, since they use the same underlying mechanism. The model of Ghahremanirad and co-workers,[37] in Figure 4a, shows two recombination pathways: direct R_{rec} and delayed by the inductor R_L. In contrast to this, the model of Moia et al., in Figure 4b, introduces a second RC line that vanishes in dc conditions. This combination of two RC branches has been applied to successfully describe the correlation of IMPS and IS spectra.[52−54] However, the circuit of Moia and co-workers[14] only allows recombination through the inductor. Their model lacks the recombination resistance R_b in Figure 1c that permits dc current when the inductor is not yet activated, at low voltage. This feature is necessary to explain the evolution of the experimental spectra with voltage, observed in Figure 1b, and the shape of the transients (refer to Figure 3a) as discussed before.

There are other models that have developed similar ideas for the interpretation of inductive features,[9,46] but they did not present an impedance function, and we do not further discuss them. On the other hand, several numerical analyses of inverted hysteresis have been proposed,[3,28,48] which is closely related to the inductive response.[29,30] All these different analyses, presented for negative capacitances and inductive hysteresis, are compatible with the general operation principle of the chemical inductor.[24,30] In fact, the first model of a chemical inductor incorporates a voltage-gated ion channel in the neuron membrane as described by Hodgkin and Huxley.[55] Therefore, the chemical inductor describes well a voltage-gated electronic current in the perovskite solar cell.[9,14,46,48]

We remark that our analysis of the transient behavior applies, more generally, to the rest of electrical and electrochemical systems showing a chemical inductor with the specific interpretation that each specific case may acquire. For example, we have shown that the chemical inductor in the halide perovskite memristor causes transients that have a form close to the natural action potential.[56] These insights can assist the formation of realistic artificial neurons with a simple device configuration.

A large number of models, related to the observation of negative capacitance/inductive impedance, have provided explanations and equivalent circuit models based on the coupling of ionic−electronic responses. The important question remains whether the observed effects can also be related to the chosen transport layers. For example, it has been observed many times that the interface between TiO_2 and perovskites gives a very large capacitance contribution that causes intense regular hysteresis,[57] and the trap passivation reduces the recombination current.[58,59] This large capacitive effect often disappears for organic contacts;[57] however, they can produce other effects such as hosting mobile ions.[60] Recently, we showed that perovskite solar cells and memristors of $MAPbI_3$ and $MAPbBr_3$ produce a predominant inverted hysteresis at high applied voltages, connected to the inductive impedance.[19,30] In Figure S3, we show the inverted hysteresis of $MAPbI_3$ devices with different contacts. Devices with TiO_2 layers show directional photocurrent, while a FTO/PEDOT:PSS/MAPI/Au memristor shows symmetrical photocurrent. In all the cases, a strong inverted hysteresis is observed in the region corresponding to intense forward bias, past V_{oc}, connected to a transition from capacitive hysteresis at low voltage to inductive control at high forward bias,[30] as remarked in Figure 1a. This confirms that the inductor is a general phenomenon occurring for different transport layers and even in nearly symmetrical devices without selective contact layers. However, the fundamental physicochemical reasons for these effects remain elusive.

In conclusion, we presented here the general theory to interpret the widespread phenomena in photocurrent transient measurements that underlie the presence of the chemical

https://doi.org/10.1021/acsenergylett.2c01252
ACS Energy Lett. 2022, 7, 2602−2610

inductor in electrical equivalent circuits of perovskite devices. We focus our attention on the famous and ubiquitous negative spike component in the time transient decays, analyzing the proportional light- and voltage-dependence of the photocurrent undershoot. From an adequate pathway to correlate independent methods (impedance responses and transient measurements), we developed a consistent analysis of a quadruple-cation perovskite-based photovoltaic device verifying that the theoretical basis is satisfied by experimental data. Our work brings a robust solution to the problem of interpretation associated with this anomalous effect observed for more than a decade in perovskite devices (solar cells, memristors that show inverted hysteresis, photodetectors, and power electronic components that respond to switching).

■ ASSOCIATED CONTENT

Supporting Information

The Supporting Information is available free of charge at https://pubs.acs.org/doi/10.1021/acsenergylett.2c01252.

Chemical inductance in impedance analysis; complete theory of the temporal relaxation processes in the perovskite inductive mode; comparison of models; inductive characteristics of perovskite devices by varying capping layers; experimental section (PDF)

■ AUTHOR INFORMATION

Corresponding Author

Enrique Hernández-Balaguera − *Escuela Superior de Ciencias Experimentales y Tecnología (ESCET), Universidad Rey Juan Carlos, 28933 Madrid, Spain;* orcid.org/0000-0002-1400-5916; Email: enrique.hernandez@urjc.es

Author

Juan Bisquert − *Institute of Advanced Materials (INAM), Universitat Jaume I, 12006 Castelló, Spain; Yonsei Frontier Lab, Yonsei University, 03722 Seoul, South Korea;* orcid.org/0000-0003-4987-4887

Complete contact information is available at: https://pubs.acs.org/10.1021/acsenergylett.2c01252

Notes

The authors declare no competing financial interest.

■ ACKNOWLEDGMENTS

This work has received funding from the Comunidad de Madrid under the SINFOTON2-CM Research Program, S2018/NMT4326-SINFOTON2-CM, and the Universidad Rey Juan Carlos (projects of reference M2417 and M2607) via "Research and development promotion Program". We thank the financial support by the Ministerio de Ciencia e Innovación of Spain (MICINN) project PID2019-107348GB-100.

■ REFERENCES

(1) Eames, C.; Frost, J. M.; Barnes, P. R. F.; O'Regan, B. C.; Walsh, A.; Islam, M. S. Ionic Transport in Hybrid Lead Iodide Perovskite Solar Cells. *Nat. Commun.* **2015**, *6* (1), 7497.

(2) Azpiroz, J. M.; Mosconi, E.; Bisquert, J.; De Angelis, F. Defect Migration in Methylammonium Lead Iodide and Its Role in Perovskite Solar Cell Operation. *Energy Environ. Sci.* **2015**, *8* (7), 2118−2127.

(3) Richardson, G.; O'Kane, S. E. J.; Niemann, R. G.; Peltola, T. A.; Foster, J. M.; Cameron, P. J.; Walker, A. B. Can Slow-Moving Ions Explain Hysteresis in the Current-Voltage Curves of Perovskite Solar Cells? *Energy Environ. Sci.* **2016**, *9* (4), 1476−1485.

(4) Calado, P.; Telford, A. M.; Bryant, D.; Li, X.; Nelson, J.; O'Regan, B. C.; Barnes, P. R. F. Evidence for Ion Migration in Hybrid Perovskite Solar Cells with Minimal Hysteresis. *Nat. Commun.* **2016**, *7*, 13831.

(5) Belisle, R. A.; Nguyen, W. H.; Bowring, A. R.; Calado, P.; Li, X.; Irvine, S. J. C.; McGehee, M. D.; Barnes, P. R. F.; O'Regan, B. C. Interpretation of Inverted Photocurrent Transients in Organic Lead Halide Perovskite Solar Cells: Proof of the Field Screening by Mobile Ions and Determination of the Space Charge Layer Widths. *Energy Environ. Sci.* **2017**, *10* (1), 192−204.

(6) Pockett, A.; Carnie, M. J. Ionic Influences on Recombination in Perovskite Solar Cells. *ACS Energy Lett.* **2017**, *2*, 1683−1689.

(7) O'Kane, S. E. J.; Richardson, G.; Pockett, A.; Niemann, R. G.; Cave, J. M.; Sakai, N.; Eperon, G. E.; Snaith, H. J.; Foster, J. M.; Cameron, P. J.; Walker, A. B. Measurement and Modelling of Dark Current Decay Transients in Perovskite Solar Cells. *J. Mater. Chem. C* **2017**, *5* (2), 452−462.

(8) Pockett, A.; Spence, M.; Thomas, S. K.; Raptis, D.; Watson, T.; Carnie, M. J. Beyond the First Quadrant: Origin of the High Frequency Intensity-Modulated Photocurrent/Photovoltage Spectroscopy Response of Perovskite Solar Cells. *Sol. RRL* **2021**, *5*, 2100159.

(9) Ebadi, F.; Taghavinia, N.; Mohammadpour, R.; Hagfeldt, A.; Tress, W. Origin of Apparent Light-Enhanced and Negative Capacitance in Perovskite Solar Cells. *Nat. Commun.* **2019**, *10* (1), 1574.

(10) Bisquert, J.; Guerrero, A. Chemical Inductor. *J. Am. Chem. Soc.* **2022**, *144* (13), 5996−6009.

(11) Mora-Seró, I.; Bisquert, J.; Fabregat-Santiago, F.; Garcia-Belmonte, G.; Zoppi, G.; Durose, K.; Proskuryakov, Y.; Oja, I.; Belaidi, A.; Dittrich, T.; Tena-Zaera, R.; Katty, A.; Lévy-Clément, C.; Barrioz, V.; Irvine, S. J. C. Implications of the Negative Capacitance Observed at Forward Bias in Nanocomposite and Polycrystalline Solar Cells. *Nano Lett.* **2006**, *6* (4), 640−650.

(12) Cole, K. S.; Baker, R. F. Longitudinal Impedance of the Squid Giant Axon. *J. Gen. Physiol.* **1941**, *24* (6), 771−788.

(13) Klotz, D. Negative Capacitance or Inductive Loop? - A General Assessment of a Common Low Frequency Impedance Feature. *Electrochem. Commun.* **2019**, *98*, 58−62.

(14) Moia, D.; Gelmetti, I.; Calado, P.; Fisher, W.; Stringer, M.; Game, O.; Hu, Y.; Docampo, P.; Lidzey, D.; Palomares, E.; Nelson, J.; Barnes, P. R. F. Ionic-to-Electronic Current Amplification in Hybrid Perovskite Solar Cells: Ionically Gated Transistor-Interface Circuit Model Explains Hysteresis and Impedance of Mixed Conducting Devices. *Energy Environ. Sci.* **2019**, *12* (4), 1296−1308.

(15) Barnett, M. W.; Larkman, P. M. The Action Potential. *Pract. Neurol.* **2007**, *7* (3), 192−197.

(16) Bou, A.; Bisquert, J. Impedance Spectroscopy Dynamics of Biological Neural Elements: From Memristors to Neurons and Synapses. *J. Phys. Chem. B* **2021**, *125* (35), 9934−9949.

(17) Xu, W.; Cho, H.; Kim, Y.-H.; Kim, Y.-T.; Wolf, C.; Park, C.-G.; Lee, T.-W. Organometal Halide Perovskite Artificial Synapses. *Adv. Mater.* **2016**, *28* (28), 5916−5922.

(18) Yang, J.-Q.; Wang, R.; Wang, Z.-P.; Ma, Q.-Y.; Mao, J.-Y.; Ren, Y.; Yang, X.; Zhou, Y.; Han, S.-T. Leaky Integrate-and-Fire Neurons Based on Perovskite Memristor for Spiking Neural Networks. *Nano Energy* **2020**, *74*, 104828.

(19) Berruet, M.; Pérez-Martínez, J. C.; Romero, B.; Gonzales, C.; Al-Mayouf, A. M.; Guerrero, A.; Bisquert, J. Physical Model for the Current-Voltage Hysteresis and Impedance of Halide Perovskite Memristors. *ACS Energy Lett.* **2022**, *7*, 1214−1222.

(20) Kirchartz, T.; Márquez, J. A.; Stolterfoht, M.; Unold, T. Photoluminescence-Based Characterization of Halide Perovskites for Photovoltaics. *Adv. Energy Mater.* **2020**, *10* (26), 1904134.

(21) Krückemeier, L.; Krogmeier, B.; Liu, Z.; Rau, U.; Kirchartz, T. Understanding Transient Photoluminescence in Halide Perovskite Layer Stacks and Solar Cells. *Adv. Energy Mater.* **2021**, *11* (19), 2003489.

(22) Futscher, M. H.; Lee, J. M.; McGovern, L.; Muscarella, L. A.; Wang, T.; Haider, M. I.; Fakharuddin, A.; Schmidt-Mende, L.; Ehrler, B. Quantification of Ion Migration in $CH_3NH_3PbI_3$ Perovskite Solar Cells by Transient Capacitance Measurements. *Mater. Horiz.* **2019**, *6* (7), 1497−1503.
(23) Tress, W.; Correa Baena, J. P.; Saliba, M.; Abate, A.; Graetzel, M. Inverted Current-Voltage Hysteresis in Mixed Perovskite Solar Cells: Polarization, Energy Barriers, and Defect Recombination. *Adv. Energy Mater.* **2016**, *6* (19), 1600396.
(24) Alvarez, A. O.; Arcas, R.; Aranda, C. A.; Bethencourt, L.; Mas-Marzá, E.; Saliba, M.; Fabregat-Santiago, F. Negative Capacitance and Inverted Hysteresis: Matching Features in Perovskite Solar Cells. *J. Phys. Chem. Lett.* **2020**, *11* (19), 8417−8423.
(25) Hernández-Balaguera, E.; Romero, B.; Najafi, M.; Galagan, Y. Analysis of Light-Enhanced Capacitance Dispersion in Perovskite Solar Cells. *Adv. Mater. Interfaces* **2022**, *9* (9), 2102275.
(26) Hernández-Balaguera, E.; del Pozo, G.; Arredondo, B.; Romero, B.; Pereyra, C.; Xie, H.; Lira-Cantú, M. Unraveling the Key Relationship Between Perovskite Capacitive Memory, Long Time-scale Cooperative Relaxation Phenomena, and Anomalous *J-V* Hysteresis. *Solar RRL* **2021**, *5* (4), 2000707.
(27) Xie, H.; Wang, Z.; Chen, Z.; Pereyra, C.; Pols, M.; Gałkowski, K.; Anaya, M.; Fu, S.; Jia, X.; Tang, P.; Kubicki, D. J.; Agarwalla, A.; Kim, H.-S.; Prochowicz, D.; Borrisé, X.; Bonn, M.; Bao, C.; Sun, X.; Zakeeruddin, S. M.; Emsley, L.; Arbiol, J.; Gao, F.; Fu, F.; Wang, H. I.; Tielrooij, K.-J.; Stranks, S. D.; Tao, S.; Grätzel, M.; Hagfeldt, A.; Lira-Cantu, M. Decoupling the Effects of Defects on Efficiency and Stability through Phosphonates in Stable Halide Perovskite Solar Cells. *Joule* **2021**, *5* (5), 1246−1266.
(28) Nemnes, G. A.; Besleaga, C.; Stancu, V.; Dogaru, D. E.; Leonat, L. N.; Pintilie, L.; Torfason, K.; Ilkov, M.; Manolescu, A.; Pintilie, I. Normal and Inverted Hysteresis in Perovskite Solar Cells. *J. Phys. Chem. C* **2017**, *121* (21), 11207−11214.
(29) Bisquert, J.; Guerrero, A.; Gonzales, C. Theory of Hysteresis in Halide Perovskites by Integration of the Equivalent Circuit. *ACS Phys. Chem. Au* **2021**, *1* (1), 25−44.
(30) Muñoz-Díaz, L.; Rosa, Á.; Bou, A.; Sánchez, R. S.; Romero, B.; John, R. A.; Kovalenko, M. V.; Guerrero, A.; Bisquert, J.; Guerrero, A. Inductive and Capacitive Hysteresis of Halide Perovskite Solar Cells and Memristors Under Illumination. *Front. Energy Res.* **2022**.
(31) Hernández-Balaguera, E.; Romero, B.; Arredondo, B.; del Pozo, G.; Najafi, M.; Galagan, Y. The Dominant Role of Memory-Based Capacitive Hysteretic Currents in Operation of Photovoltaic Perovskites. *Nano Energy* **2020**, *78*, 105398.
(32) Hernández-Balaguera, E.; Polo, J. L. On the Potential-Step Hold Time When the Transient-Current Response Exhibits a Mittag-Leffler Decay. *J. Electroanal. Chem.* **2020**, *856*, 113631.
(33) Fabregat-Santiago, F.; Kulbak, M.; Zohar, A.; Vallés-Pelarda, M.; Hodes, G.; Cahen, D.; Mora-Seró, I. Deleterious Effect of Negative Capacitance on the Performance of Halide Perovskite Solar Cells. *ACS Energy Lett.* **2017**, *2* (9), 2007−2013.
(34) Guerrero, A.; Bisquert, J.; Garcia-Belmonte, G. Impedance Spectroscopy of Metal Halide Perovskite Solar Cells from the Perspective of Equivalent Circuits. *Chem. Rev.* **2021**, *121* (23), 14430−14484.
(35) Ogata, K. *Modern Control Engineering*, 5th ed.; Prentice Hall, 2010.
(36) Guerrero, A.; Garcia-Belmonte, G.; Mora-Sero, I.; Bisquert, J.; Kang, Y. S.; Jacobsson, T. J.; Correa-Baena, J.-P.; Hagfeldt, A. Properties of Contact and Bulk Impedances in Hybrid Lead Halide Perovskite Solar Cells Including Inductive Loop Elements. *J. Phys. Chem. C* **2016**, *120* (15), 8023−8032.
(37) Ghahremanirad, E.; Bou, A.; Olyaee, S.; Bisquert, J. Inductive Loop in the Impedance Response of Perovskite Solar Cells Explained by Surface Polarization Model. *J. Phys. Chem. Lett.* **2017**, *8* (7), 1402−1406.
(38) von Hauff, E.; Klotz, D. Impedance Spectroscopy for Perovskite Solar Cells: Characterisation, Analysis, and Diagnosis. *J. Mater. Chem. C* **2022**, *10* (2), 742−761.
(39) Bisquert, J. Hopf Bifurcations in Electrochemical, Neuronal, and Semiconductor Systems Analysis by Impedance Spectroscopy. *Appl. Phys. Rev.* **2022**, *9*, 011318.
(40) Dualeh, A.; Moehl, T.; Tétreault, N.; Teuscher, J.; Gao, P.; Nazeeruddin, M. K.; Grätzel, M. Impedance Spectroscopic Analysis of Lead Iodide Perovskite-Sensitized Solid-State Solar Cells. *ACS Nano* **2014**, *8* (1), 362−373.
(41) Khan, M. T.; Huang, P.; Almohammedi, A.; Kazim, S.; Ahmad, S. Mechanistic Origin and Unlocking of Negative Capacitance in Perovskites Solar Cells. *iScience* **2021**, *24*, 102024.
(42) Sanchez, R. S.; Gonzalez-Pedro, V.; Lee, J.-W.; Park, N.-G.; Kang, Y. S.; Mora-Sero, I.; Bisquert, J. Slow Dynamic Processes in Lead Halide Perovskite Solar Cells. Characteristic Times and Hysteresis. *J. Phys. Chem. Lett.* **2014**, *5* (13), 2357−2363.
(43) Ravishankar, S.; Almora, O.; Echeverría-Arrondo, C.; Ghahremanirad, E.; Aranda, C.; Guerrero, A.; Fabregat-Santiago, F.; Zaban, A.; Garcia-Belmonte, G.; Bisquert, J. Surface Polarization Model for the Dynamic Hysteresis of Perovskite Solar Cells. *J. Phys. Chem. Lett.* **2017**, *8* (5), 915−921.
(44) Pockett, A.; Eperon, G. E.; Sakai, N.; Snaith, H. J.; Peter, L. M.; Cameron, P. J. Microseconds, Milliseconds and Seconds: Deconvoluting the Dynamic Behaviour of Planar Perovskite Solar Cells. *Phys. Chem. Chem. Phys.* **2017**, *19* (8), 5959−5970.
(45) Kumar, R.; Kumar, J.; Srivastava, P.; Moghe, D.; Kabra, D.; Bag, M. Unveiling the Morphology Effect on the Negative Capacitance and Large Ideality Factor in Perovskite Light-Emitting Diodes. *ACS Appl. Mater. Interfaces* **2020**, *12* (30), 34265−34273.
(46) Jacobs, D. A.; Shen, H.; Pfeffer, F.; Peng, J.; White, T. P.; Beck, F. J.; Catchpole, K. R. The Two Faces of Capacitance: New Interpretations for Electrical Impedance Measurements of Perovskite Solar Cells and Their Relation to Hysteresis. *J. Appl. Phys.* **2018**, *124*, 225702.
(47) Choi, W.; Song, S. W.; Han, S. G.; Cho, K. The Origin of Photoinduced Capacitance in Perovskite Solar Cells: Beyond Ionic-to-Electronic Current Amplification. *Adv. Electron. Mater.* **2020**, *6* (6), 2000030.
(48) Shen, H.; Jacobs, D. A.; Wu, Y.; Duong, T.; Peng, J.; Wen, X.; Fu, X.; Karuturi, S. K.; White, T. P.; Weber, K.; Catchpole, K. R. Inverted Hysteresis in $CH_3NH_3PbI_3$ Solar Cells: Role of Stoichiometry and Band Alignment. *J. Phys. Chem. Lett.* **2017**, *8* (12), 2672−2680.
(49) Kovalenko, A.; Pospisil, J.; Krajcovic, J.; Weiter, M.; Guerrero, A.; García-Belmonte, G. Interface Inductive Currents and Carrier Injection in Hybrid Perovskite Single Crystals. *Appl. Phys. Lett.* **2017**, *111*, 163504.
(50) Tong, C.-J.; Cai, X.; Zhu, A.-Y.; Liu, L.-M.; Prezhdo, O. V. How Hole Injection Accelerates Both Ion Migration and Nonradiative Recombination in Metal Halide Perovskites. *J. Am. Chem. Soc.* **2022**, *144* (14), 6604−6612.
(51) Dhifaoui, H.; Harindu Hemasiri, N.; Aloui, W.; Bouazizi, A.; Kazim, S.; Ahmad, S. An Approach to Quantify the Negative Capacitance Features in a Triple-Cation based Perovskite Solar Cells. *Adv. Mater. Interfaces* **2021**, *8* (22), 2101002.
(52) Afroz, M. A.; Aranda, C. A.; Tailor, N. K.; Yukta; Yadav, P.; Tavakoli, M. M.; Saliba, M.; Satapathi, S. Impedance Spectroscopy for Metal Halide Perovskite Single Crystals: Recent Advances, Challenges, and Solutions. *ACS Energy Lett.* **2021**, *6* (9), 3275−3286.
(53) Ravishankar, S.; Aranda, C.; Sanchez, S.; Bisquert, J.; Saliba, M.; Garcia-Belmonte, G. Perovskite Solar Cell Modeling Using Light- and Voltage-Modulated Techniques. *J. Phys. Chem. C* **2019**, *123* (11), 6444−6449.
(54) Bou, A.; Pockett, A.; Raptis, D.; Watson, T.; Carnie, M. J.; Bisquert, J. Beyond Impedance Spectroscopy of Perovskite Solar Cells: Insights from the Spectral Correlation of the Electrooptical Frequency Techniques. *J. Phys. Chem. Lett.* **2020**, *11* (20), 8654−8659.
(55) Hodgkin, A. L.; Huxley, A. F. A Quantitative Description of Membrane Current and Its Application to Conduction and Excitation in Nerve. *J. Physiol.* **1952**, *117* (4), 500−544.

https://doi.org/10.1021/acsenergylett.2c01252
ACS Energy Lett. 2022, 7, 2602−2610

(56) Bisquert, J.; Guerrero, A. Dynamic Instability and Time Domain Response of a Model Halide Perovskite Memristor for Artificial Neurons. *J. Phys. Chem. Lett.* **2022**, *13* (17), 3789−3795.
(57) Kim, H.-S.; Jang, I.-H.; Ahn, N.; Choi, M.; Guerrero, A.; Bisquert, J.; Park, N.-G. Control of *I-V* Hysteresis in $CH_3NH_3PbI_3$ Perovskite Solar Cell. *J. Phys. Chem. Lett.* **2015**, *6* (22), 4633−4639.
(58) Tan, H.; Jain, A.; Voznyy, O.; Lan, X.; García de Arquer, F. P.; Fan, J. Z.; Quintero-Bermúdez, R.; Yuan, M.; Zhang, B.; Zhao, Y.; Fan, F.; Li, P.; Quan, L. N.; Zhao, Y.; Lu, Z.-H.; Yang, Z.; Hoogland, S.; Sargent, E. H. Efficient and Stable Solution-Processed Planar Perovskite Solar Cells Via Contact Passivation. *Science* **2017**, *355* (6326), 722−726.
(59) Yan, Y.; Liu, C.; Yang, Y.; Hu, G.; Tiwari, V.; Jiang, D.; Peng, W.; Jha, A.; Duan, H.-G.; Tellkamp, F.; Ding, Y.; Shi, W.; Yuan, S.; Miller, D.; Ma, W.; Zhao, J. Fundamental Flaw in the Current Construction of the TiO_2 Electron Transport Layer of Perovskite Solar Cells and Its Elimination. *ACS Appl. Mater. Interfaces* **2021**, *13* (33), 39371−39378.
(60) Rombach, F. M.; Haque, S. A.; Macdonald, T. J. Lessons Learned from Spiro-OMeTAD and PTAA in Perovskite Solar Cells. *Energy Environ. Sci.* **2021**, *14*, 5161−5190.

https://doi.org/10.1021/acsenergylett.2c01252
ACS Energy Lett. 2022, 7, 2602−2610